Indian J. Phys **75B** (2), 79–84 (2001)

I J P B
an international journal

Dynamical structure of planetary nebulae in three dimensions : a numerical solution

J Ghanbari
Department of Physics, University of Ferdowsi, Mashhad, Iran
and
A R Khesali*
Department of Physics, University of Mazandaran, Babolsar, Iran
E-mail khesali@umcc.ac.ir

Received 20 July 2000, accepted 7 February 2001

Abstract The interacting two winds model and a nonspherical density function in three dimensions is introduced to study the dynamical structure of planetary nebulae. A fast wind with a mechanical energy interacts with a super wind with mass-loss rate of $2 \times 10^{-5} \frac{M_\odot}{yr}$ and a velocity of 10 km/s. As a result, it produces a dense and luminous medium.

Keywords Planetary nebulae, ISM dynamics, numerical solution

PACS Nos. 98.38.Am, 98.38.Ly

1. Introduction

The idea that the planetary nebulae (PNe) originate from the outer atmosphere of red giants, goes back to Shklovski [1]. Later on Goldreich and Abell [2] argued convincingly that red giants are the most probable proginators of PNe and that they are therefore, shells of gaseous material that have been lost in the recent past by their central stars. Their old central stars are hotter than galactic O stars, 5×10^4 K° – 3×10^5 K°, and less luminous, $M_v = -3$ to 5. The expanding shells have a typical velocity of 25 km/s. As a consequence of the shell expansion, the shell density decreases which causes the nebular emission to decrease as well and therefore, they rapidly become unobservable. Observed PNe have densities in the range of $5 \times 10^2 - 10^4$ cm ^{3}, and typical masses in the order of $0.1 - 1.0\, M_\odot$. The study of PNe is important in several different fields in astronomy. As low density objects, generally transparent to radiation extending longwards from the Lyman limit to radio wavelengths, they furnish excellent examples for the study of physical processes in dilute gases subjected to photoionization by a central star source. Since their formation must be a significant event in the evolution of a large number of stars, a study of PNe and associated stars can give important information on some aspects of the late stage of stellar evolution. The aim of the theoretical work is to explain the dynamical structures of PNe. Pikelner [3], Kwok [4], and Kahn [5] among others, presented one dimensional models to explain the dynamics of round PNe, choosing a spherical density distribution for the red giant envelope (RGE). Kahn and West [6] gives a simplified two dimensional model for a non-spherical density function. Ghanbari [7] gives a two dimensional model to calculate the structure of the shell. Recently, Bobrowsky [8] and Lopez [9] study the PNe in two dimensions.

2. The density

Since the RGE density function is the main feature for study the PNe shapes, Ghanbari [7] used a non-uniform density function for RGE to calculate the physical parameters of non-spherical PNe in terms of time. He assumed the red giant mass-loss rate per steradian which depends on the polar angle θ.

$$\rho(r,\theta) = \frac{\dot{m}_{sw}(1+\varepsilon \sin^n \theta)}{B v_{sw} r^2} \qquad (1)$$

* Corresponding Author

where $B = \int_0^{4\pi}(1+\varepsilon\sin^n\theta)d\omega$, $\dot{m}_{sw}$ and $v_{sw}(\sim 10$ km/s) are the slow wind mass-loss rate and velocity respectively, which are independent of time and space, and integer n and parameter ε are free quantities which change density distribution functions. For the following reasons, the non-spherical density distribution, depends on both polar angle θ and azimutal angle ϕ. (i) Some of the central strars of PNe can be one member of binary stars. Then the shape of the central star can be deformed from spherical to the shape of the ball of American football, because of mass transfer [10]. (ii) If the direction of the magnetic field of the cer.tral star is non-uniform, then the ejection of matter from the magnetic poles of the star would be different from that of the other regions. With these assumptions, we choose the density of the red giant's envelope, to have the following θ and ϕ dependences

$$\rho(r,\theta,\phi) = \frac{\dot{m}_{sw}(1+\varepsilon\sin^n\theta)(1+\varepsilon'\sin^{n'}\phi)}{v_w r^2\int_0^{2\pi}\int_0^{\pi}(1+\varepsilon\sin^n\theta)(1+\varepsilon'\sin^{n'}\phi)\sin\theta d\theta d\phi} \quad (2)$$

where ε' and n' are two parameters which affect on the distribution of mass in the azimuth angle ϕ. As we see in this case, the density has its minimum value at $\theta = \phi = 0$ and it will have its maximum value at equatore when $\phi = \pi/2$.

3. The shell dynamics

It is now widely thought that the interaction of the fast wind with a mass-loss rate $\dot{m}_{fw} \sim 10^{-7} - 10^{-8}\, M_\odot/yr$ and a velocity $v_{sw} \sim 10$ km/s, can explain the evolution of a PNe [11]. The interaction sets up the usual two shock flow patterns with four distinct regions, and three distinct boundaries that represent the site of the interaction and the regions beyond it (Figure 1). The inward shock S_1 decelerates the stellar wind and the outward shock S_2 accelerates the ambient gas. The

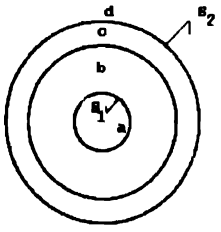

Figure 1. Shock flow pattern with distinct regions and boundaries

shocked stellar wind region has a sound speed of the order of 1000 km/s. As long as the shell is expanding at a velocity which is typically ~20 – 50 km/s, less than the sound speed 1000 km/s, the bubble pressure P_w is uniform in space but changes in time. If we make the assumption that the stream lines are radial and the shock is strong, then the equation of motion of a shell element follows from the momentum consideration. We also neglect both the ram pressure in the radial direction of the shell element and the centrifugal pressure correction term [12]. For a shell element of mass dM_s and radial velocity $\dot{R}_s$ at time t, the equation of motion in the radial direction is

$$\frac{d}{dt}\left((\dot{R}_s - v_{sw})dM_s\right) = P_w dA_s\cos\alpha\,, \quad (3)$$

where dA_s is the surface element of the shell and angle $\alpha\left(\equiv \arctan\left(\frac{1}{R}\frac{\partial R_s}{\partial\theta}\right)\right.$ is the directional angle of the surface element at position R_s between the radius and the normal to the surface at the same point (Figure 2). Since the contribution

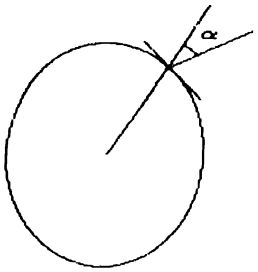

Figure 2. Directional angle α of the surface element

of the stellar wind to the mass flux is negligible relative to the contribution of the slow wind [13], the rate of the inflow mass to the cone of semi angle β is

$$\frac{d}{dt}(dM_s) = \int_0^{\beta}\rho(\dot{R}_s - v_{sw})dA_s\,, \quad (4)$$

$$\frac{dM_s}{dA_s}\dot{R}_s + \rho(\dot{R}_s - v_{sw})^2 = P_w\cos\alpha\,, \quad (5)$$

the important parameter defining the properties of the fast wind is the output rate of the central stars wind mechanical energy, $L_w = \frac{1}{2}\dot{m}_{fw}v_{fw}^2$. As we noted before, the energy content of the shocked wind region is almost entirely in the form of thermal energy. The thermal energy per unit volume of a monoatomic gas is equal to $\frac{3}{2}$ times the gas pressure. The total thermal energy of the region therefore, equals $\frac{3}{2}P_wV$, where V is the bubble volume. Concentration of energy for this region which is in thermal equilibrium, demands that

$$\frac{d}{dt}\left(\frac{3}{2}P_wV\right) = L_w - P_w\frac{dV}{dt}\,. \quad (6)$$

The eq. (6) states that the rate of change of thermal energy of a hot shocked region is equal to the rate at which energy is fed into the region by fast wind minus the rate at which the hot gas does work on the interstellar gas. If we define the bubble volume $V = \frac{1}{3}\int_0^{2\pi}R_s^3\sin\theta d\theta d\phi$ and assume a uniform pressure P_w, then the energy equation (6) gives

$$P_w = \frac{2tL_w}{5t\left(\int_0^{2\pi}\int_0^{\pi}\dot{R}_sR_s^2\sin\theta d\theta d\phi - 2\int_0^{2\pi}\int_0^{\pi}R_s^3\sin\theta d\theta d\phi\right)}\,. \quad (7)$$

4. The solution

To solve the equation of motion in order to find radius, velocity and other physical parameter of the nebular shell, we have at time $t = -\tau - t_0$, the superwind terminates and τ years later, a physical change occurs and a fast wind begins. The interaction between the two winds occurs at time $t = 0$, *i e* t_0 years later. The time-scale t_0 is given by

$$t_0 = \frac{R_{rg} + v_{sw}\tau}{v_{fw} - v_{sw}}, \tag{8}$$

where R_{rg} is the red giant radius which is typically $100 R_\odot$. We assume that the shell motion obeys the similarity solution of $R_s = R_0 + \lambda v_{sw} t$ and $\dot{R}_s = \lambda v_{sw}$ at the early stages of the interaction. $R_0 = R_{rg} + v_{sw}(\tau + t_0)$ is the shell radius at time $t = 0$ and λ is a parameter which determines the initial velocity of the shell and is therefore related to the input energy L_w by the fast wind. Since $v_{fw} \gg v_{sw}$, then $R_0 = R_{rg} + v_{sw}\left(\tau + \frac{R_{rg} + v_{sw}\tau}{v_{fw} - v_{sw}}\right) \simeq R_{rg} + v_{sw}\tau$ which is much larger than the red giant radius R_{rg} even for small values of time-scale τ which could be small as a few year. During these stages, the density has a spherical distribution of $\rho(R_s) = \frac{\dot{m}_{sw}}{4\pi v_{sw} R_s^2}$. Putting the initial values of R_s and $\dot{R}_s$ in eq. (5), the bubble pressure at the early stage is

$$P_s = \left(\frac{\lambda - 1}{\lambda}\right)^2 \frac{m_s}{4\pi v_{sw} t^2}. \tag{9}$$

There are several parameters which determine the shape of the shell. $\dot{m}_{sw}$, ε, ε' and n, n' change the RGE density, and λ affects the fast wind energy rate. Another parameter which changes the initial shell radius is the time-scale τ. If the backward shock has a radius R_1 in the early stages, then assuming the inner shock velocity $\dot{R}_1 << v_{fw}$, this is called hot shock. The density in the hot shocked medium is

$$\rho = \frac{\dot{m}_{fw} t}{\frac{4}{3}\pi R_s^3} \cdot \frac{3}{4\pi} \frac{m_{fw}}{\lambda^3 v_{sw}^3 t^2} \tag{10}$$

This gives a temperature of

$$T = \frac{\mu \bar{m}}{} \frac{P_w}{}. \tag{11}$$

Putting the typical values in eq. (11), $T \simeq 4 \times 10^7$ K. Such a hot gas can be treated as an adiabatic medium with a cooling time t_c which is given by Kahn [14], as

$$t_c = \frac{P_w^{\frac{3}{2}}}{q\rho^{\frac{5}{2}}} \tag{12}$$

where the parameter $q = 4 \times 10^{32}$ cm^6 gm^{-1} s^{-4} is given for normal cosmic abundances. On the other hand, this high temperature provides a large sound speed $c_b \sim 400$ km s^{-1} and the sound corssing time $\tau_c = \frac{R_s - R_1}{c_b} \simeq \frac{R_s}{c_b}$ is much less than the dynamical time-scale, this region therefore has a uniform pressure. The gas does not cool effectively if

$$\frac{P_w^{\frac{2}{5}}}{\rho^{\frac{2}{5}}} >> q t_c \text{ [5] or}$$

$$t_c >> 20 \frac{\dot{m}_{fw} q}{\lambda^3 v_{sw}^3 v_{fw}} \tag{13}$$

i.e., for $\lambda = 3$ and the previous values of the other parameters, $t_c \gg 3.7\, yr$. This puts a lower limit for the time-scale τ. Since this limit is very small compared with the typical dynamical time-scale of PNe, it does not have any appreciable effect on the shell structure. τ may have an upper limit upto the dynamical time-scale of PNe ($\sim 10^4\, yr$).

5. The results

Numerical calculations have been achieved by a program written in Matlab enviornment. We have used Matlab's subroutins to solve the differential equations and to calculate the integrals which have been discussed in the previous sections. For our models which are considered to be in thermal equilibrium, we adopted $\dot{m}_{sw} = 2 \times 10^{-5} M_\odot yr^{-1}$, v_{sw} = 10 km s^{-1}. As was pointed out in Section 4, $t_0 \simeq 0$ and R_0 can be ignored and the energy driven mode is applicable at most stages of the evolution. Here, we have examined the effects of different parameters on the shape and physical quantities of the shell. As λ increases, the wind mechanical energy increases and therefore the wind puts more energy into the bubble. If the other parameters are kept constant, the shell velocity increases in both polar and equatorial directions for all ϕ angles. This can be seen in Figures 3 and 4, for

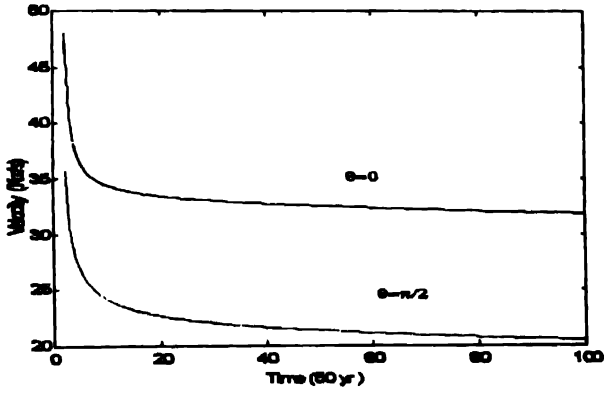

Figure 3. Velocity as a function of time at $\phi = 90°$ for two different values of θ, ($\theta = 0$, $\theta = \pi/2$); the parameters are to be $\varepsilon = 1$, $\varepsilon' = 1$, $\lambda = 3$, $n = 2$, $n' = 2$

$\phi = 90°$, as λ changes from 3 to 6. Moreover, at the same conditions as we can see from Figures 5 and 6, changing λ from 3 to 6 causes the shell radius to increase and the shell thickness to decrease for example, in the equatoral plane

($\theta = 90°$) and for $\phi = 90°$. As a result, we conclude that the thin shell approximation has been a suitable assumption. There are four parameters $\varepsilon, \varepsilon', n, n'$ which affect the density contrast. As long as λ is taken constant, $\varepsilon, \varepsilon', n, n'$ change only the distribution of the slow wind density in the medium. As n and n' are taken constant and ε and ε' change from 1 to 10, the shape of the shell becomes more elongated along the polar direction and a bulge appears around the equator (compare Figures 7 and 8). On the other hand when $\phi = 0$ or *phi* = 180° we will have cusp at the equator (compare Figures 9 and 10). As n increases, we will

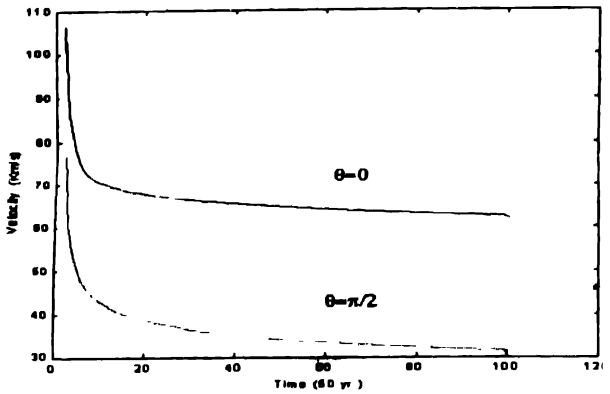

Figure 4. Velocity as a function of time at $\phi = 90°$ for two different values of θ, ($\theta = 0$, $\theta = \pi/2$); the parameters are chosen to be $\varepsilon = 1$, $\varepsilon' = 1$, $\lambda = 6$, $n = 2$, $n' = 2$.

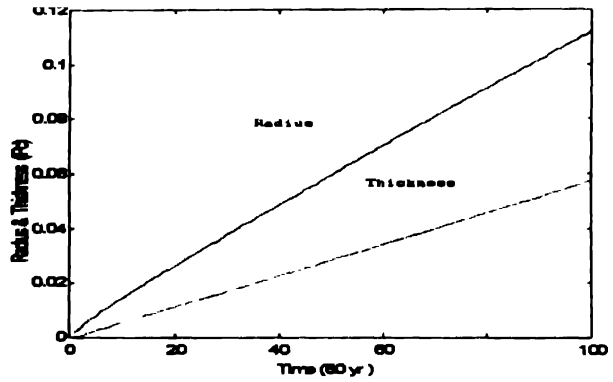

Figure 5. Radius and thickness as a function of time at $\theta = 90°$ and $\phi = 90°$, the parameters are chosen to be $\varepsilon = 1$, $\varepsilon' = 1$, $\lambda = 3$, $n = 2$, $n' = 2$

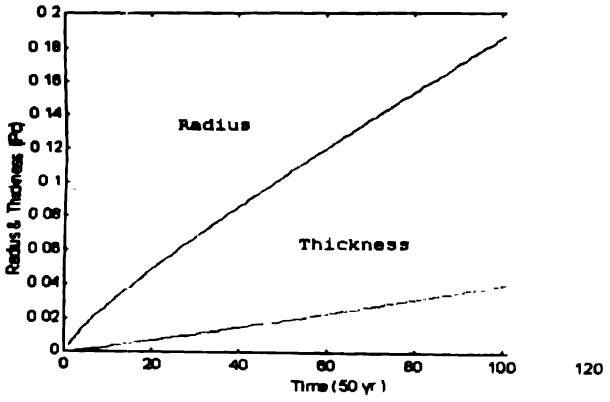

Figure 6. Radius and thickness as a function of time at $\theta = 90°$ and $\phi = 90°$, the parameters are chosen to be $\varepsilon = 1$, $\varepsilon' = 1$, $\lambda = 6$, $n = 2$, $n' = 2$

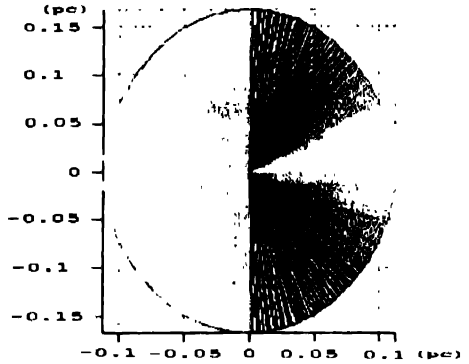

Figure 7. PNe cross section in the azimutal directions $\phi = 90°$ (left) and $\phi = 270°$ (right), θ changes from 0 to 180°. The parameters are $\varepsilon = 1$, $\varepsilon' = 1$, $\lambda = 3$, $n = 2$, $n' = 2$

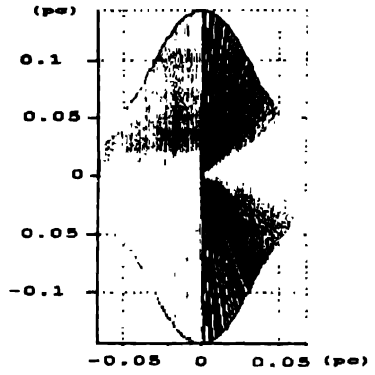

Figure 8. PNe cross section in the azimutal directions $\phi = 90°$ (left) and $\phi = 270°$ (right), θ changes from 0 to 180°. The parameters are $\varepsilon = 10$, $\varepsilon' = 10$, $\lambda = 3$, $n = 2$, $n' = 2$

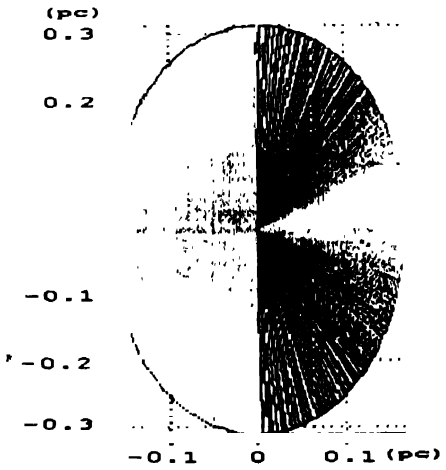

Figure 9. PNe cross section in the azimutal directions $\phi = 0°$ (left) and $\phi = 180°$ (right), θ changes from 0 to 180°. The parameters are $\varepsilon = 1$, $\varepsilon' = 1$, $\lambda = 3$, $n = 2$, $n' = 2$.

have more and more mass concentration at the equator and simultaneously less and less mass concentration at the pole. Similarly, the larger value of n' means that the concentration of mass at direction $\phi = 90$ is maximum and the concentration at $\phi = 0$ is minimum. Figures 11 and 12 show how changes

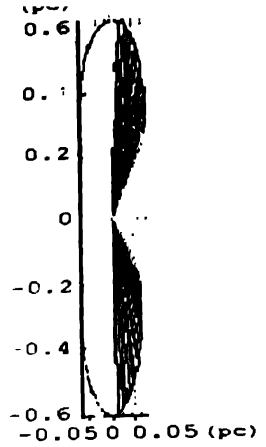

Figure 10. PNe cross section in the azimutal directions $\phi = 0°$ (left) and $\phi = 180°$ (right), θ changes from 0 to 180°. The parameters are $\varepsilon = 10$, $\varepsilon' = 10$, $\lambda = 3$, $n = 2$, $n' = 2$.

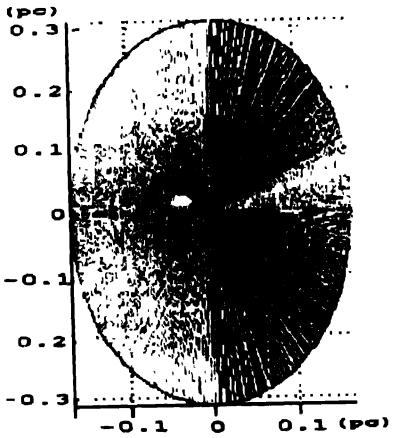

Figure 11. PNe cross section in the azimutal directions $\phi = 0°$ (left) and $\phi = 180°$ (right), θ changes from 0 to 180°. The parameters are $\varepsilon = 1$, $\varepsilon' = 1$, $\lambda = 3$, $n = 2$, $n' = 2$.

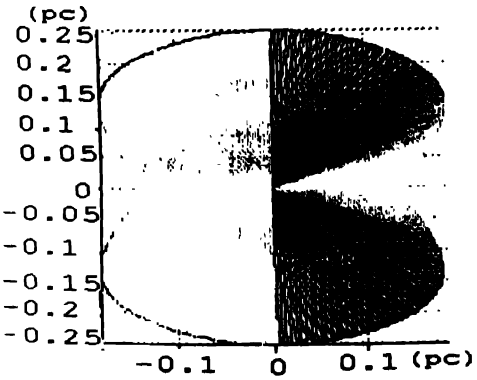

Figure 12. PNe cross section in the azimutal directions $\phi = 0°$ (left) and $\phi = 180°$ (right), θ changes from 0 to 180°. The parameters are $\varepsilon = 1$, $\varepsilon' = 1$, $\lambda = 3$, $n = 10$, $n' = 10$.

of n from 2 to 10, causes the shapes along the equator start to make cusp and the radius around the pole to remain constant. Figures 13 and 14 show when n' changes from

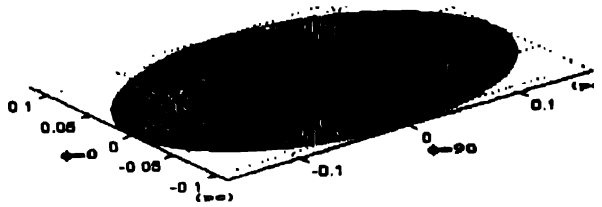

Figure 13. PNe cross section at $\theta = 90°$, ϕ changes from 0 to 360°, the parameters are $\varepsilon = 1$, $\varepsilon' = 1$, $\lambda = 3$, $n = 2$, $n' = 2$.

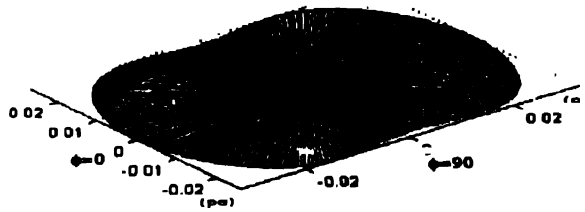

Figure 14. PNe cross section at $\theta = 90°$, ϕ changes from 0 to 360°, the parameters are $\varepsilon = 1$, $\varepsilon' = 1$, $\lambda = 3$, $n = 2$, $n' = 10$.

2 to 10, shapes along $\phi = 90$ start to make cusp and radius will remain constant around $\phi = 0$. As the final results, Figures 15 and 16 show the surface changes in three

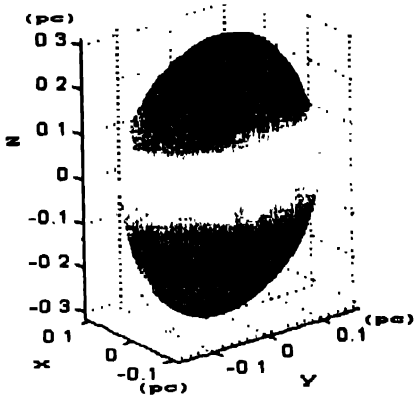

Figure 15. PNe surface for $\varepsilon = 1$, $\varepsilon' = 1$, $\lambda = 3$, $n = 2$, $n' = 2$.

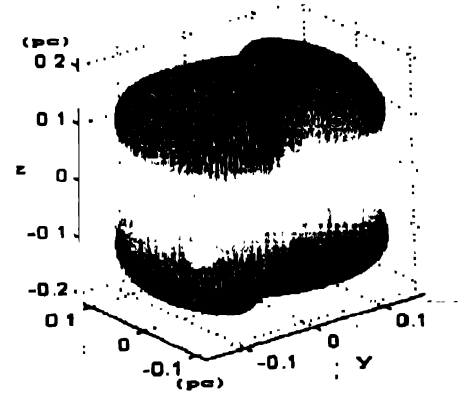

Figure 16. PNe surface for $\varepsilon = 1$, $\varepsilon' = 1$, $\lambda = 3$, $n = 10$, $n' = 10$.

dimensions corresponding to changes of n, n' from 2 to 10. This method of numerical analysis of dynamical structures has been proved to have high capabilities and our future work will be to study the ionization structure of planetary nebulae.

References

[1] I A Shklovski *Ast.* **33** 315 (1956)

[2] P Goldreich and G O Abell *Publ Astron. Soc Pac.* **78** 232 (1966)

[3] S B Pikelner *Astrophys J Lett* **15** 91 (1973)

[4] S Kwok *J Roy Astron Soc Can.* **74** 216 (1980)

[5] F D Kahn *Planetary Nebulae* (ed) D R Flower *IAU Symp* No. **103** p305 (1983)

[6] F D Kahn and K A West *Mon. Not. Roy. Astron. Soc.* **212** 83 (1985)

[7] J Ghanbari *Structure of Wind Nebulae* (PhD Thesis) (1989)

[8] M Bobrowsky *Nature. 2 April* (1998)

[9] J A Lopez and R Vazqez *Astron. J.* (1999)

[10] Z Kopal *Close Binary Systems* (Netherland : Reidel) (1959)

[11] A Renzini in *Physical Processes in Red Giants* (eds.) I Iben and A Renzini (Dordrecht : Reidel) p431 (1981)

[12] J L Giuliani (Jr) *Astrophys. J.* **256** 624 (1982)

[13] J E Dyson *Astrophys. Space Sci.* **35** 299 (1975)

[14] F D Kahn *Astron Astrophys* **50** 145 (1976)